

Magnetically responsive gels based on crosslinked gelatin: An overview on the synthesis, properties, and their potential in water remediation

Maria Fernanda Horst, Mario Daniel Ninago & Verónica Lassalle

To cite this article: Maria Fernanda Horst, Mario Daniel Ninago & Verónica Lassalle (2017): Magnetically responsive gels based on crosslinked gelatin: An overview on the synthesis, properties, and their potential in water remediation, International Journal of Polymeric Materials and Polymeric Biomaterials, DOI: [10.1080/00914037.2017.1362640](https://doi.org/10.1080/00914037.2017.1362640)

To link to this article: <http://dx.doi.org/10.1080/00914037.2017.1362640>



Accepted author version posted online: 10 Aug 2017.
Published online: 10 Aug 2017.



Submit your article to this journal [↗](#)



Article views: 7



View related articles [↗](#)



View Crossmark data [↗](#)

Magnetically responsive gels based on crosslinked gelatin: An overview on the synthesis, properties, and their potential in water remediation

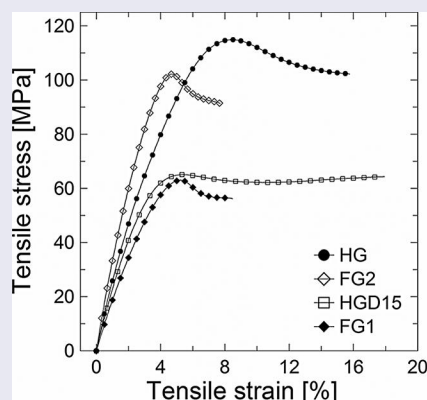
Maria Fernanda Horst^a, Mario Daniel Ninago^b and Verónica Lassalle^a

^aINQUISUR-CONICET-UNS, Departamento de Química, Bahía Blanca, Buenos Aires, Argentina; ^bPLAPIQUI-CONICET-UNS, Departamento de Ingeniería Química, Bahía Blanca, Buenos Aires, Argentina

ABSTRACT

Efficient adsorbent ferrogels based on gelatin and dextrose were synthesized using freeze-thawing technique. Two different methodologies of magnetic particles incorporation were developed. An exhaustive morphologic and thermal characterization of hydro and ferrogels was achieved. The performance of ferrogel in water remediation was tested using Cd(II) as model contaminant. The adsorption ability was evaluated as a function of pH, initial heavy metal concentration, and contact time. The maximum adsorption capacity was 35 mg of Cd(II)/g of adsorbent. Ferrogel was regenerated by washing with distilled water, maintaining efficiency of almost 30% after the fourth cycle.

GRAPHICAL ABSTRACT



ARTICLE HISTORY

Received 30 March 2017
Accepted 29 July 2017

KEYWORDS

Adsorption; ferrogel; gelatin; heavy metals; water remediation

1. Introduction

Owing to two specific properties, such as biocompatibility and biodegradability, biopolymeric-based hydrogels represent a class of materials with potential to be applied in several fields such as medicine, pharmacy, biology, agriculture, etc [1,2]. Biopolymers-based hydrogels are widely study for environmental applications, especially chitosan, polyglutamic acid, and crosslinked hydrogels based on the mentioned biopolymers [3–6].

In particular, gelatin hydrogels have found diverse specific uses in biomedicine during last years [7–10].

The main limitation associated with gelatin hydrogel is that it exhibits poor mechanical properties and readily dissolves in water in a short time at temperatures above 29°C. Therefore, the crosslinking treatment must be necessarily implemented to obtain suitable materials regarding their applications [11]. Consequently, physical and chemical crosslinking procedures


have been developed using different agents that is, glutaraldehyde, gellan gum, genipin, among other polymers [10,12,13].

Besides, during the last few years, hybrid materials based on polymeric gel and inorganic moieties have received increasing attention due to the synergic effect of both components in terms of providing specific properties to the prepared materials.

In particular, magnetic hydrogel emerged as efficient tools in fields such as bioseparation, biomedical, and catalytic [14–16]. Regarding gelatin magnetic hydrogel, it was difficult to find any article in the literature exploring their application for environmental remediation. However, there are many researches based on gelatin ferrogel, reporting their synthesis methodology and release behavior oriented to biomedical application [17–21]. In most of these articles, ferrogels were prepared co-precipitating magnetic nanoparticles in the medium of hydrogel formation. Moreover, in some works,

CONTACT Maria Fernanda Horst  mfhorst@uns.edu.ar  Dra. María Fernanda Horst, INQUISUR-CONICET-UNS, Av. Alem 1253, B8000CPB, Bahía Blanca, Buenos Aires, Argentina.

Color versions of one or more of the figures in the article can be found online at www.tandfonline.com/gpom.

 Supplemental data for this article can be accessed at [\[publisher's weblink\]](http://publisher's weblink).

authors have used biopolymers such as chitosan and used carbodiimide to induce the crosslinking structure [19,20].

The aim of this manuscript is to obtain gelatin-based magnetic gels able to be efficiently used as adsorbents of water pollutants. The combination of the high adsorption capacity with the magnetic properties results in a versatile reusable material with wide industrial interest.

Dextrose was selected as crosslinking agent, evaluating different concentrations. The hydrogel preparation method was the freeze-thawing (F-T). Besides, two routes for the incorporation of magnetic nanoparticles were analyzed.

After a survey of available literature, it was difficult to find reports dealing with the preparation of gelatin-based magnetic gel crosslinked with dextrose and without using any triggered for the reaction.

Furthermore, an exhaustive characterization of hydro and magnetic gelatin gels was achieved, determining swelling, thermal, magnetic and mechanical properties, and surface morphology. Finally, their performance as adsorbent was evaluated in batch experiments, using a standard solution of cadmium ion as model of water contaminant. An in-depth study on the adsorption behavior was performed covering the influence of pH media, contact time, and heavy metal ion concentration. Moreover, an intensive study of material regeneration and reuse was performed to assess the feasibility to apply the adsorbent in a continuous industrial process.

Finally, it is important to highlight that, to the best of these authors' knowledge, the use of gelatin-based hydrogel for remediation applications is very limited, at least judging by the available articles. More specifically, the combination of substrates, synthesis methodology, and application here proposed has not been earlier reported in open literature.

2. Materials and methods

Gelatin was purchased from Fluka Analytical (Sigma-Aldrich). It is 48723 Gelatin tested according Ph. Eur (CAS No.: 9000-70-8). Dextrose anhydre, $M_w = 180.16 \text{ g mol}^{-1}$, was from Anedra (Argentina) and was used as reinforcement of hydrogel gelatin network. Iron(II) sulfate, heptahydrated, and iron(III) chloride, hexahydrated, were purchased from Cicarelli Laboratory (Argentina). 0.1 M NaOH solution from Cicarelli. Distilled water was used for the preparation of all reactant solutions. Standard solutions of cadmium between 0.5 and 400 mg L^{-1} were used for the adsorption assays.

2.1. Hydrogels synthesis

Gelatin (10% w/v) and different amounts of dextrose (5, 15, and 50% w/w) were used for hydrogel synthesis using the freeze-thawing methodology. The technique consists of dissolved biopolymers in water and allows to swell for 24 h at 6°C. After that, a homogenous solution was obtained by increasing the temperature at 50°C for 1 h. Finally, varied volumes of solution were filled in disposable base molds and allowed to form the gel at room temperature. The obtained hydrogels were named as gelatin-dextrose hydrogel (HGD) (5, 15, and 50 refer to content dextrose).

2.2. Synthesis of ferrogels

Gelatin/dextrose hydrogel HGD15 was selected for the preparation of ferrogels. This selection was based on the swelling degree and the stability on the application conditions.

Two different methodologies of synthesis were assayed to obtain the ferrogels. One was the in situ mineralization of magnetite nanoparticles in gelatin preformed hydrogel through co-precipitation. For this purpose, one portion of gelatin hydrogel was introduced in a $\text{Fe}^{3+}/\text{Fe}^{2+}$ (2:1 molar ratio) aqueous solution during 24 h at room temperature. Then, the iron-loaded hydrogel was placed in 0.1 M NaOH solution during 150 min. After this period of time, ferrogel was washed several times to remove the NaOH present in the surface and other moieties of the reaction.

The second methodology involved a gelatin/dextrose solution that was allowed to swell with a homogenous concentrated dispersion of Fe_3O_4 nanoparticles at 6°C for 24 h. The used Fe_3O_4 nanoparticles were previously synthesized in our laboratory by conventional co-precipitation method earlier reported [22]. Then, the solution was heated at 50°C for 1 h, filled in appropriate molds and allowed to form the ferrogel there. Figure 1 depicts the schematic representation of the synthesis methodology of ferrogels. In Figure 1a, a photograph of the ferrogel obtained through the first methodology (here in after, FG1) may be observed. The magnetic ferrogel prepared by the second methodology (here in after, FG2) may be appreciated in Figure 1b.

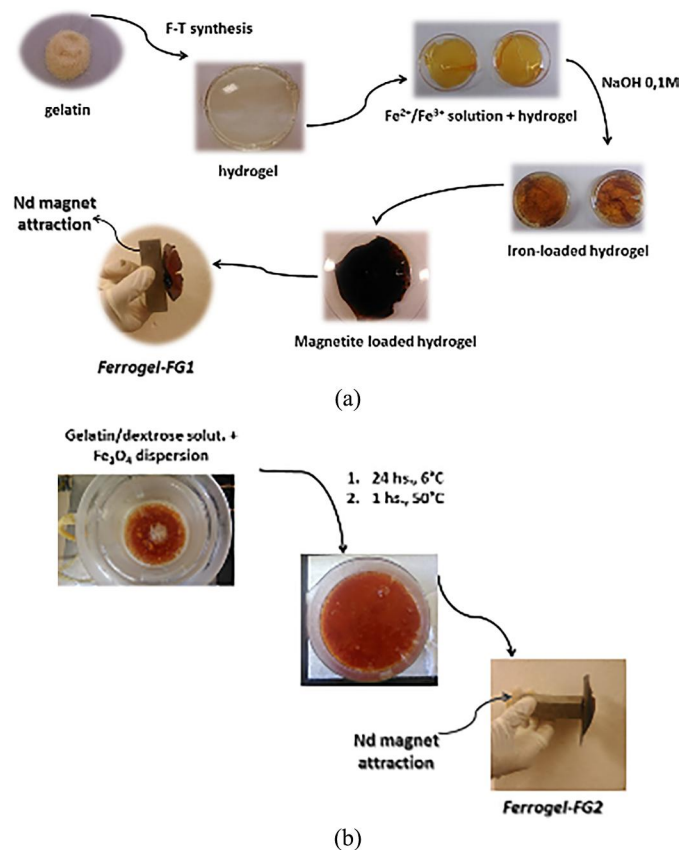


Figure 1. Schematic representation of steps involves in ferrogels synthesis.

3. Characterization techniques

3.1. FTIR spectroscopy, X-ray diffraction, and electron microscopy

Fourier transforms infrared spectroscopy (FTIR) of hydro and ferrogels were recorded on a Thermo Scientific Nicolet iS50 FT-IR, modulo NIR: Thermo Scientific Nicolet iS50 NIR module with Integrating Sphere in the frequency range of 4,000–400 cm^{-1} .

X-ray diffraction (XRD) analyses were performed to confirm the crystalline structure of magnetite nanoparticles on the ferrogels.

A scanning electron microscope (SEM) was used to examine morphologies (SEM LEO EVO 40-XVP). Dehydrated hydrogels and ferrogel were cryo-fractured in liquid nitrogen, then gold metalized for the surface analysis.

3.2. Thermogravimetric techniques

The mineral content of the ferrogels was determined by thermal degradation (TGA). The TGA measurements were carried out in a TA Instrument Discovery Series. Samples were heated from 30 to 700°C at 10°C min^{-1} , using nitrogen as flux (25 mL min^{-1}). Curves of weight loss as function of the temperature were recorded and the maximum decomposition temperature of each component was obtained from first derivative curves.

Thermal properties of films were studied by DSC using a Pyris 1 PerkinElmer apparatus. Temperature and heat of fusion were calibrated using pure indium metal as a standard reference. Approximately, 0.01 g of sample was used. All materials were heated from 20 to 140°C at 10°C min^{-1} to obtain the glass transition temperature (T_g) and the melting point temperature (T_m).

3.3. Swelling assays

Swelling studies were carried out in distilled water at room temperature. The pH values of water samples assayed were from 6 to 7, and may be considered similar to real polluted water sample. Air-dried cross sections of gelatin hydro and ferrogels were weighed in the dry state. The samples were left swelling in water in a closed vessel. The excess of water of each sample was removed with a filter paper before weighing. All samples were weighed after a certain amount of time until equilibrium swelling was reached. The swelling equilibrium degree (SD%) was determined as:

$$\text{SD\%} = \frac{(W_f - W_i)}{W_i} \times 100 \quad (1)$$

where W_i is the initial weight of the samples before the immersion and W_f is the final weight of the samples at water content equilibrium.

3.4. Mechanical tests

The uniaxial stress–strain curves of the free-standing gelatin films were obtained using an Instron tensile tester with humidity and temperature controlled in unconfined module.

The tensile tests were performed in a universal mechanical machine Instron 3369, with a 1 kN load cell, in accordance with the ASTM D882-02 guidelines. The tensile specimens were cut in rectangular shapes with dimensions of 50 mm in length and 6.5 mm in width. The gauge length was fixed at 25 mm and the cross head speed was 5 mm min^{-1} at room temperature. All tests were carried out on a minimum of five samples and the reported results are average values. The tensile moduli, break elongation, and break strength were also obtained.

3.5. Magnetic measurements

Magnetic properties were measured with a commercial vibrating sample magnetometer at room temperature with a magnetic field in the –10 to 10 kOe range.

3.6. Adsorption assays

Adsorption tests of heavy metal ions on hydro and ferrogels were performed in batch using Cd(II) solutions as model heavy metal. In a typical experience, an amount of hydrogel matrix and ferrogel was kept in contact with heavy metal solution. It was let swollen in this media for a certain period of time at room temperature. Aliquots of the solution were withdrawn to measure the concentration of remained metal ion by atomic absorption spectroscopy using a GBC Avanta 932. The adsorbed amount was calculated as follows:

$$q(t) = \frac{(C_0 - C_t)}{m} V \quad (2)$$

where C_0 and C_t (mg) are the initial amount of metal ion and the amount of metal ion unadsorbed in the solution, respectively; V is the volume of the Cd(II) 100 mg L^{-1} solution; and m is the mass of adsorbent material.

3.6.1. Effect of pH

The effect of pH on the efficiency of cadmium adsorption was investigated in the HGD15, FG1, and FG2. The pH of the heavy metal solution was adjusted at 3.0 and 7.0, using 1 M HCl or NaOH, respectively. To do this, 20 mg of each material was contacted with 20 mL of Cd(II) solution of about 100 mg L^{-1} . Aliquots of 2 mL were taken after 2 h of immersion. The remained heavy metal ion was measured by absorption spectroscopy and the amount of removed cadmium was calculated Eq. 2.

3.6.2. Effect of contact time

The effect of contact time of the cadmium with the ferrogel was carried out by placing 100 mg of magnetic adsorbent in a flask containing 100 mL of Cd(II) solution of about 100 mg L^{-1} at pH 7. The ferrogels were allowed swelling in the media and aliquots were withdrawn at different times during 3 h. Experimental data were fitted with pseudo-first-order and pseudo-second-order kinetic models to predict the adsorption kinetics. The pseudo-first-order equation was represented by:

$$\frac{1}{q_t} = \frac{k_1}{q_e} + \frac{1}{q_e} \quad (3)$$

where k_1 is the pseudo-first-order rate constant (min^{-1}) of adsorption and q_e and q_t are the amounts of metal ion adsorbed at equilibrium and time t (min), respectively. The value of $1/q_t$ was calculated from experimental results and plotted against $1/t$ (min^{-1}).

The linear form of pseudo-second-order equation can be written as:

$$\frac{1}{q_t} = \frac{1}{k_2 q_e^2} + \left(\frac{1}{q_e}\right)t \quad (4)$$

where k_2 is the pseudo-second-order rate constant of adsorption ($\text{g mg}^{-1} \text{min}^{-1}$).

3.6.3. Effect of initial concentration

The effect of the initial concentration of cadmium ion on the uptake of ferrogel was carried out by placing 30 mg of adsorbent material in a series of flasks containing 30 mL of Cd(II) solution with concentrations in the range of 0.5–400 mg L^{-1} at pH 7. The ferrogel was allowed swelling in the solution for 30 min at room temperature. The unadsorbed heavy metal ion was measured by absorption spectroscopy and the amount of adsorbed cadmium was calculated Eq. 2.

3.7. Regeneration and reuse of ferrogel

Studies of regeneration and reusability of ferrogels were performed using Cd(II) aqueous solutions.

To do this, 100 mg of ferrogel was contacted with 100 mL 50 mg L^{-1} of heavy metal solution at pH 7 during 30 min. Cd-loaded ferrogel was immersed in water for 10 min and repeating the procedure four times with refresh aqueous solution each time to assess the adsorbent purification. Then, the material was contacted with the same cadmium solution used in the first adsorption contact assay. This procedure of adsorption–desorption–adsorption was repeated three times. The amount of cadmium ion adsorbed and/or desorbed in each procedure described above was monitored by atomic absorption spectroscopy.

4. Results and discussion

4.1. Characterization of hydro and ferrogels

The incorporation of crosslinking agent was required to reach materials stable enough under the applications conditions.

To investigate the possibility of structural changes in gelatin molecules in hydrogels due to interactions with dextrose (crosslinking agent) and to corroborate the presence of magnetite nanoparticles, FTIR spectroscopy was performed. Figure 2 shows the FTIR spectra of hydrogel and FG. The spectroscopic analysis of hydrogel matrix revealed the main peaks corresponding to gelatin structure. It clearly distinguished the amide I band, between 1,500 and 1,700 cm^{-1} corresponding to the amide I and amide II. These bands correspond to common protein structure associated with stretching vibrations of C=O bond, coupling bending of N–H bond and stretching of C–N [23,24]. The presence of dextrose could not be corroborated because of its typical bands that were not distinguished. It is probable that they overlapped

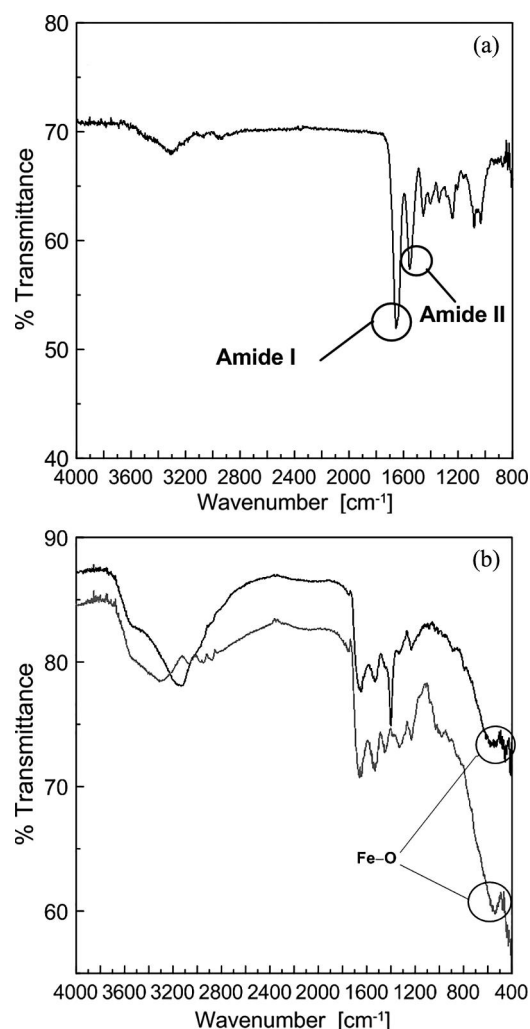


Figure 2. FTIR spectra of (a) HG (dark line) and HGD15 (grey line), and (b) FG1 (dark line) and FG2 (grey line). Note: HGD, gelatin–dextrose hydrogel; FTIR, Fourier transforms infrared.

with the corresponding to gelatin functional groups. However, the efficient dextrose role as crosslinker may be corroborated by the stability (swelling) assays as well as mechanical properties later presented. In fact, it is known that interactions through aldehyde groups from dextrose and amine groups of gelatin would take place allowing the crosslinking [25].

The spectra of FG1 and FG2 displayed changes in the region of amide I and amide II bands. This could be probably due to the interaction of magnetic nanoparticles with gelatin hydrogel matrix. A shift on the wavelength values of amide I and amide II groups from gelatin was observed in another work after incorporation of magnetic particles into biopolymeric matrix [26]. In this study, the authors attributed these changes to the electrostatic interaction between amide bond and the magnetic particles. This may be considered as evidence of structural changes in gelatin hydrogel, indicative of order of the triple-helix state [24]. Moreover, the interaction of iron oxide with O–H groups from gelatin was also evident, since hydroxyl group bonding extends and the broadness of the 3,600–3,200 cm^{-1} region band decreases (Figure 2).

Furthermore, a characteristic absorption peak of iron oxide (Fe–O) was observed near 600 cm^{-1} in both ferrogel spectra.

This confirmed that magnetite nanoparticles were successfully incorporated into gelatin hydrogel matrix.

4.2. XRD data

The crystallographic characterization of hydrogel matrix and ferrogels was analyzed by XRD measurements (see Supplementary Material). The diffractogram of hydrogel showed a broad peak at about $2\theta \sim 20^\circ$ and a small peak at $2\theta \sim 8$, which may be ascribed to crystalline structure of gelatin [27].

The presence of spinel phase of Fe_3O_4 clearly alters the pattern of raw polymer. The peaks associated with the crystalline planes of magnetite are evidenced at 30° , 35° , 43° , and 57° of 2θ values in both ferrogels corresponding to the scattering of lattices (2,2,0), (3,1,1), (4,0,0), and (5,1,1) of magnetite, respectively [22]. The iron oxide peaks in FG2 diffractogram appear narrower than the similar peaks in FG1 diffractogram. Besides, the intensity of these peaks has more pronounced in FG2 than FG1. This discrepancy may be ascribed to differences in the procedure of Magnetic nanoparticles (MNPs) crystallization when they were directly co-precipitated in the polymeric matrix. Another factor able to generate these differences is the magnetic core size. The direct co-precipitation may induce higher aggregation with clusters around 300 nm composed of small particles. This was confirmed by scanning microscopy images. These data reveal that direct co-precipitation methodology may induce higher aggregation than the procedure involving pre-formed MNPs.

4.3. SEM microscopy

The morphology of dried gelatin crosslinked hydro and ferrogels was analyzed by SEM, and the obtained images are depicted in Figure 3. This technique was used to visualize differences in the gelatin hydrogel network structure with the crosslinking agent and before and after the magnetite loading. The samples analyzed were dried at room temperature, which leads to a contracted porous material.

The SEM images of raw gelatin hydrogel (Figures 3a and 3b) displayed a highly macroporous sponge-like structure with an average mesh size about $2 \mu\text{m}$. Different surfaces are observed in crosslinked gelatin hydrogels, as suggest in Figures 3c and 3d. More smoothly, surfaces were found when gelatin hydrogel was synthesized in the presence of dextrose. The incorporation of the crosslinking agent reduced the porosity of the surface. The less presence of porous is independent of the dextrose nominal concentration.

Regarding ferrogels morphology, the images display a smooth surface with clusters of very small particles, lower than approx. 300 nm in size (Figures 3e and 3f). Comparing the ferrogel surface with hydrogel, it is observed that the former exhibits smaller pore size or even a less porous morphology, and therefore a denser hydrogel network. For FG1, it was observed that zones with high aggregation of MNPs appear as clusters. Meanwhile, FG2 displayed homogenously dispersed particles forming smaller clusters than in FG1. These results are in accordance with the methodology of incorporation the magnetic nanoparticles.

4.4. Thermal properties

Thermal properties of hydrogels with different dextrose content and ferrogels were measured by DSC. Figure 4a shows the first heating scan of neat gelatin hydrogel HG, hydrogel crosslinked HGD15, and the ferrogels (FG1 and FG2). The thermal parameters were analyzed. DSC curves for HG show two thermal transitions: The first one is the corresponding to the glass transition temperature $\sim 69.3^\circ\text{C}$ where the polysaccharide chains starting to move and slide independently of the other chains, thus rendering them more flexible and deformable. The second at 102°C is associated with the melting partial triple-helix structure of gelatin [28]. The HGD15 matrix showed only one thermal transition corresponding to T_g temperature. This fact could be attributed to the presence of dextrose that acted as plasticizer agent. Besides, T_g value for HGD15 was 10°C lower than the obtained for neat gelatin. This behavior could be associated with the formation of amorphous gelatin structure. Several authors reported similar values of T_g for amorphous gelatin [28–30]. For all hydrogel matrices, T_g values were reduced and more pronounced for the hydrogel with the higher dextrose concentration.

The use of lower nominal amounts of dextrose did not produce the expected reduction in T_g values, being similar to those corresponding to neat gelatin. On the other hand, for FG1 and FG2, the glass transition temperatures values were similar to those obtained for HGD15 matrix. These results suggest that the incorporation of magnetite nanoparticles did not affect T_g value.

4.5. Thermal degradation

Thermogravimetric measurements were used to evaluate degradation processes of the obtained materials as a function of temperature and to obtain the final mineral content on synthesized ferrogel. TGA and first derivative curves of hydrogels matrices and ferromagnetic hydrogels are shown in Figure 4b. Thermograms of gelatin hydrogel matrix HG and crosslinked hydrogel matrix HGD15 are in accordance with those reported by several authors [31,32]. For HG and HGD15 matrices, two weight loss steps were observed. Both matrices presented an initial weight loss, corresponding to samples dehydration, up to 155°C . According to Jurikova et al. [33], the high water content is the result of the water molecules diffusion within the matrix through hydrogen bonds with hydroxyl groups of glucosyl units, resulting a weight loss around 8%. The second degradation step in the temperature range of $250\text{--}350^\circ\text{C}$ with mass loss of 80% corresponds to the organic breakdown of polysaccharide chains and finally about 10% of the initial mass remained as a residue (Figure 4a). In Figure 4 also, two ferrogels (FG1 and FG2) are included. Similarly, in FG1 and FG2 thermograms, events related to water evaporation were detected [34]. Particularly, the most significant decomposition stage occurs at $\sim 325^\circ\text{C}$ and this degradation could be associated with the decomposition of polysaccharide chains and it can be appreciated from the first derivatives curves (Figure 4c), (mass loss $\sim 75\%$). Similar results were reported by several authors [32–35]. Finally, about 25% of the initial mass remained as a mixture of organic

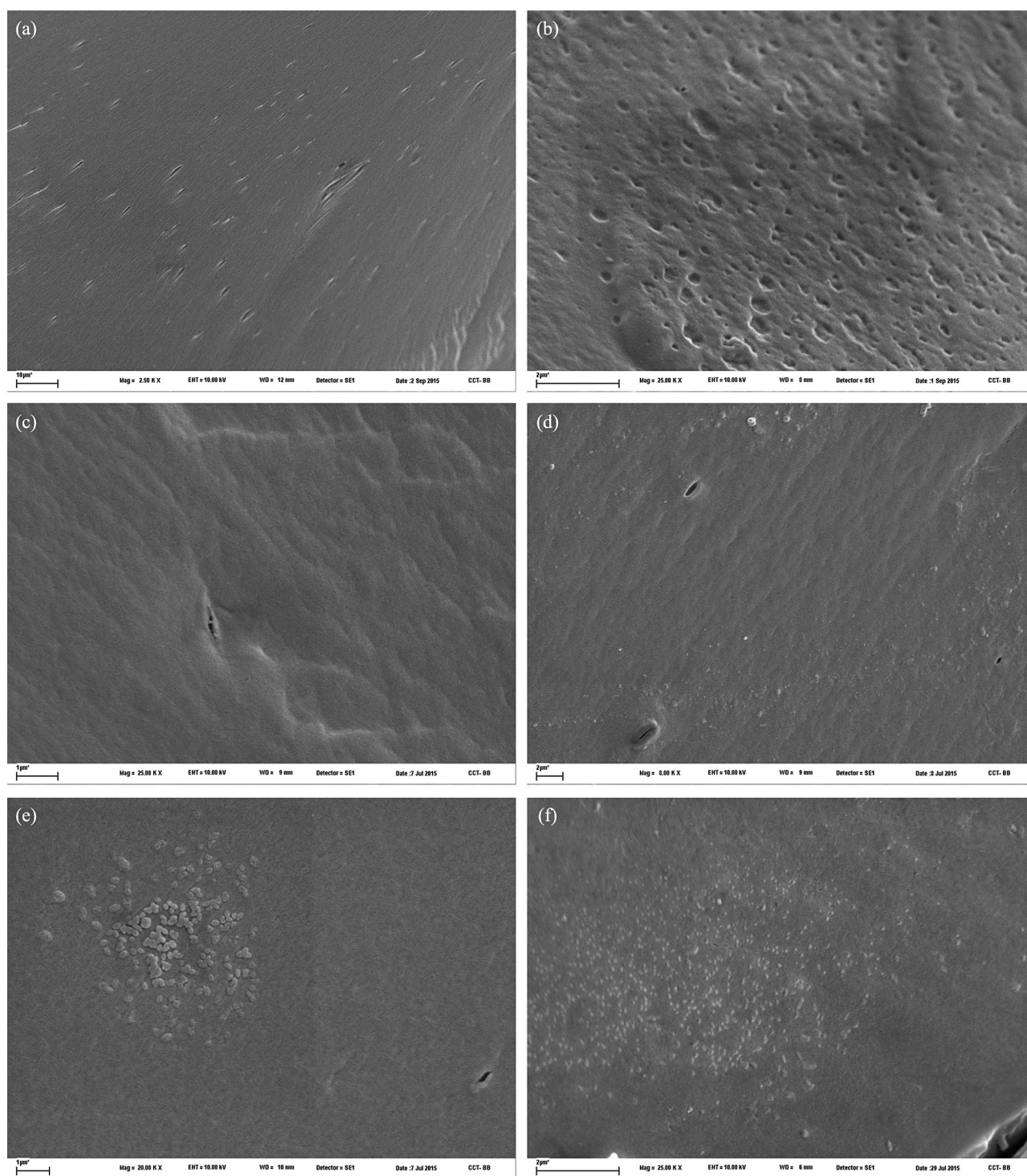


Figure 3. SEM images of (a) HG at 2,500 \times , (b) HG at 25,000 \times , (c) HGD15 at 25,000 \times , (d) HGD50 at 8,000 \times , (e) FG1 at 20,000 \times , and (f) FG2 at 25,000 \times . *Note:* HGD, gelatin–dextrose hydrogel; SEM, scanning electron microscope.

residue and magnetic nanoparticles incorporated to the hydrogel matrix. As it can be observed, magnetite incorporation did not produce significant changes in the thermal stability of the hydrogel matrices.

4.6. Ferrogels composition

The composition of ferrogel, in terms of magnetite content, may be further estimated by atomic absorption spectroscopy

(AA) expressed as Fe concentration. The recovered data indicated that FG1 exhibits 10% w/w of magnetite, whereas FG2 7% w/w. Therefore, by combining these information with the corresponding to thermogravimetric measurements, it is possible to infer that from the 25% of mass lost, around 10% corresponds to magnetite in the ferrogels. Hence, roughly 15% could be attributed to organic moieties residue. Considering the initial amount of magnetic nanoparticles used for FG2 synthesis, almost 15% of the total mass was successfully

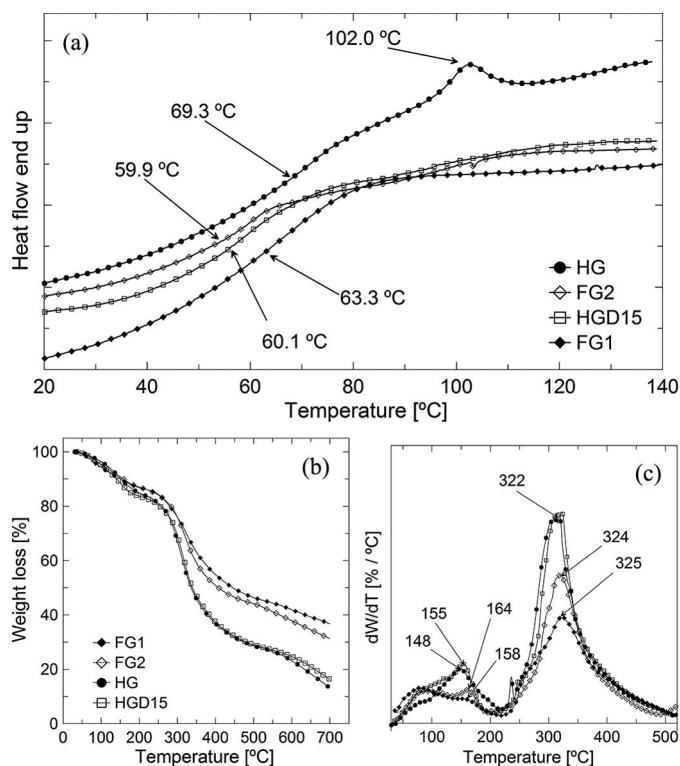


Figure 4. (a) DSC curves of neat gelatin, hydrogel gelatin matrix HGD15, and ferromagnetic hydrogels (FG1 and FG2). (b) TGA curves of HG, HGD15, FG1, and FG2. (c) First derivative TGA curves. Note: HGD, gelatin–dextrose hydrogel.

incorporated and remain linked in the ferrogel matrix. Moreover, from this analysis, it emerges that *in situ* co-precipitation method ensures higher levels of MNPs incorporation.

4.7. Tensile properties of films

The tensile modulus vs break strain was plotted from films of hydrogel matrices (HG and HGD15) as well as synthesized FG1 and FG2. The obtained curves are included in Supplementary Material and the mechanical properties are summarized in Table 1. Regarding to the hydrogel matrices, maximum tensile stress of HG was 30% higher than the dextrose crosslinked matrix (HGD15). Although it is known that crosslinking reaction occurs between $-\text{CHO}$ of dextrose dialdehydes and $-\text{NH}_2$ of the gelatin matrix, the pH ~ 7 used during the synthesis of HGD15 could lead to a decrease in active sites of crosslinking reaction, producing a decline in their mechanical behavior [36]. However, the maximum tensile strain was not affected. Respect to FG1, the maximum tensile stress was shifted to lower values (5%) regarding to HGD15 matrix. These results evidenced that different functions of the MNPs, regarding to the FGs mechanical properties, are found depending on the methodology followed to MNPs incorporation.

Table 1. Mechanical properties of the hydrogel matrices and ferrogels.

Sample	σ (MPa)	E (MPa)	ε (%)
HG10	109.4 ± 7.8	2467.4 ± 211.5	14.6 ± 1.7
HGD15	72.6 ± 10.0	2647.8 ± 336.2	16.4 ± 2.2
FG1	69.2 ± 8.7	2590.1 ± 91.1	8.1 ± 0.6
FG2	60.4 ± 12.0	3133.1 ± 707.5	8.4 ± 0.2

When the *in situ* co-precipitation of magnetite was performed, substantial enhancement of the mechanical properties was not reached. However, FG2 showed an increase in 18% in the maximum elastic modulus compared with HGD15. This reveals a reinforcement action of the magnetic particles in the hydrogel matrix when the synthesis is mediated by pre-formed MNPs.

On the other hand, the maximum tensile strain was significantly affected, producing a reduction of 50% and 48% compared to HGD15. This effect could be associated with the possible aggregation of magnetic particles and the increase size of the filling, leading to a reduction of this mechanical property. Similar results were found in a study of the mechanical properties of hydrogels [28] and gelatin composites reinforced with mineral clays [32].

4.8. Magnetic measurements

The magnetization behavior (per mass unit of ferrogel) as a function of the applied magnetic field in FG1 and FG2 was examined at different temperatures. The obtained magnetization curves are shown in Figure 5. FG1 (Figure 5a) presents superparamagnetic behavior until ~ 100 K ($M(T)$ and $M(H)$ curves were reversible) where the larger particles begin to block showing irreversibility in both $M(T)$ and hysteresis loops. The saturation magnetization is low, roughly 20 emu/g, compared with bulk magnetite (roughly 80 emu/g). This could be attributed to the smaller size of the particles and the presence of the gelatin matrix which wrapped around the magnetic nanoparticles. This behavior was observed in other systems. For example, Jia et al. [37] prepared chitosan magnetic nanoparticles and observed 11.15 emu/g of saturation magnetization. Furthermore, Chen et al. [26] synthesized magnetic gelatin spheres crosslinked with glutaraldehyde and they observed superparamagnetism behavior and M_s of 32.7 emu/g and displayed 90–100 nm size value measured by TEM.

For FG1 $M(T)$ curves and making the derivative respect to temperature: $f(T) = T \cdot d(M_z f_c(T) - M_f c(T))/dT$, this function is proportional to the temperature blocking distribution or barrier energy or volume of nanoparticles (taking into account a magnetic anisotropy constant of 5×10^5 erg/cm³). Assuming spherical size of particles, the volume distribution can be estimated as size distribution. This assumption results in 4.5 nm for particle size (Figure 5b). It is important to highlight that the value estimated from this analysis correspond to magnetic core instead the value given by SEM analysis which correspond to magnetite core and the enclosing composed of gel matrix.

On the other hand, different behavior displayed FG2 respect to magnetization measured. The magnetic particles of this ferrogel seems to be much larger and represent irreversibility at room temperature in both $M(T)$ and the hysteresis loops (Figure 5c). In this case, the particles sizes, of about 35 nm approximately, seem to be much larger than in FG1. Taking into account that the size is determined from estimation, these sizes are consistent with those determined by TEM in previous works [39]. The M_s was 30 emu/g, approximately. In spite of their larger sizes, these MNPs still remain low M_s values, and this fact may be ascribed to the low crystallinity.

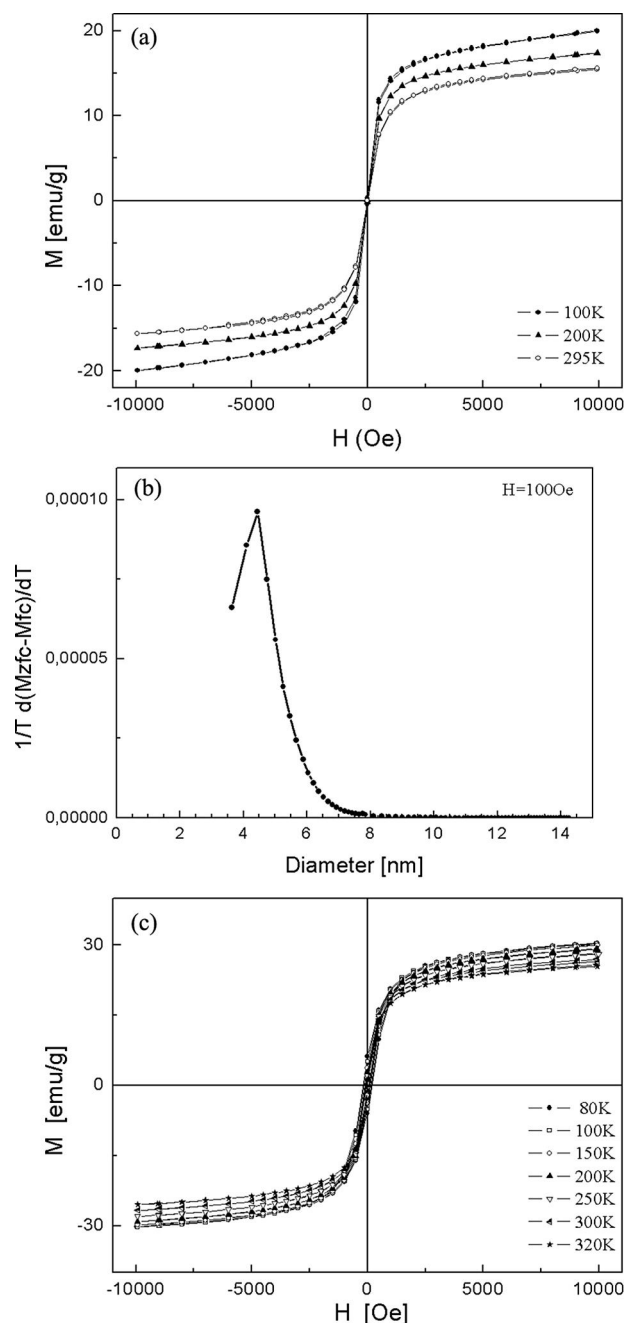


Figure 5. (a) FG1 and (c) FG2 M vs H cycles obtained from dehydrated ferrogels samples at several temperatures, (b) size distribution.

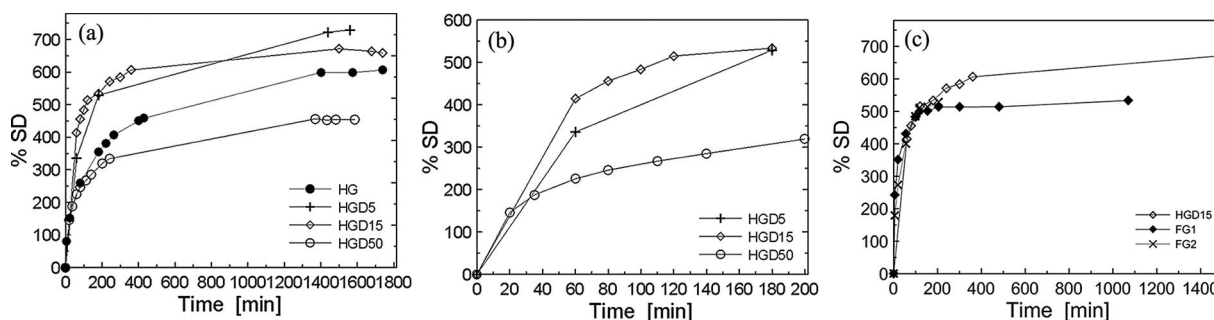


Figure 6. Swelling assays as a function of time in an aqueous solution (a and b) HG and HG matrixes (c) HGD15, FG1, and FG2. Note: HGD, gelatin–dextrose hydrogel.

4.9. Swelling studies

Swelling behavior of hydro and ferrogels is an important parameter regarding their application as adsorbent of pollutants in aqueous media or in biomedical field such as tissue engineering. Swelling increases the pore size and thus facilitates migration of different moieties inside the matrix. Figure 6a depicts the swelling profile of gelatin hydrogel crosslinked with different concentrations of dextrose at different storage time in distilled water. The swelling percentage of non-crosslinked gelatin hydrogel is about 450% after 6 h. The maximum water content was reached at 24 h of storage in water.

A decrease in the swelling% was observed as a function of the dextrose concentration, after crosslinking. The maximum swelling percentage registered was 700% for HGD5. Although HGD15 displayed less swelling%, 670%, this material was further selected as hydrogel matrix for the synthesis of ferrogels. This selection was done taking into account that this hydrogel exhibited maximum water uptake during the first 2 h reaching SD% of 500 (Figure 6b). Crosslinked hydrogels exhibit reduced chain mobility due to the intramolecular interactions; and thus it could influence the water sorption and swelling performance. As dextrose content increased, more intermolecular associations in gelatin hydrogel between functional groups of gelatin and dextrose could be achieved. This behavior may be justified assuming that an increment of dextrose mass leads a decrease in the swelling%.

It is important to highlight that the stability of HGD in water was maintained for almost 24 h, exceeding this time hydrogels undergo mass loss and consequently disintegration. Hence, this behavior reveals that gelatin crosslinked with dextrose resulted in hydrogel with weak linkages, as it was observed in tensile assays. Therefore, neat hydrogel would not be a suitable material to water remediation.

Different response was observed when swelling behavior of ferrogels was analyzed (Figure 6c). FG1 was stored in water for 7 days without loss of stability. In fact, a partial dissolution was observed near 10 days of incubation in water. The maximum swelling% was 500%.

In the case of FG2, it exhibited poor stability in water, reaching only 4 h without mass loss, exceeding this time gel dissolution was observed.

It is evident that swelling degree decreases with the presence of magnetic nanoparticles, comparing with the hydrogel matrix. This behavior may be justified by changes in the

internal structure of preformed hydrogel by means of *in situ* formed MNPs (FG1) [37,38].

The presence of iron oxides particles inside the hydrogel could contribute to the reinforcement of its internal structure probably acting as point of crosslinking (Figures 3e and 3f). This enables an increase in the stability in water and was probably due to interactions between the gelatin amine groups of hydrogel which can act as iron binding. Similar behavior was previously observed by Helminger et al. [18] in gelatin magnetic hydrogel where the presence of magnetic nanoparticles onto the polymeric matrix influences and limits the swelling behavior of ferrogel [18].

4.10. Performance of hydro and ferrogels as adsorbents of heavy metals in water

The performance of FGs as adsorbents was evaluated in batch using a Cd(II) aqueous solution. Some factors influencing the adsorption process were tested based on previous own works [39]. Assays were also conducting using the HGD15 as reference. In all the cases, the ratio ferrogel/Cd(II) was fixed in 1:1 meaning e.g., 100 mL of heavy metal ion solution per 100 mg of ferrogel. Although the adsorbent dose probably affects the adsorption process, this parameter was not evaluated at this stage of this research.

4.10.1. Effect of pH

Selected pHs were 3 and 7 based on the values commonly found in real water samples; in these conditions, cadmium remains available as ion. The formation of insoluble hydroxide occurs at pHs higher than 8 [39].

The recovered data, expressed as mg of heavy metal ion adsorbed/g of adsorbent material, are included in Figure 7a. From the figure, it is observed that at pH = 3 the three materials exhibit almost similar adsorption capability. The values, expressed as % of removed Cd with respect to the total available, were 40% for HGD15 and 41% for FG1 and FG2. Meanwhile, at pH = 7, 91%, 83%, and 86% were registered using FG1, FG2, and HGD15, respectively.

Gelatin structure is composed of several amino acids [40]. So, COO⁻ and NH₂⁻ functional groups are the responsible for cadmium adsorption. It is possible that at higher pH the carboxylate groups of gelatin could act as linkage points for

Cd ions. In accordance with the adsorption performance of materials in the two different pH analyzed, pH = 7 was chosen as the optimum value for the following assays. It is important to highlight that at this pH, FG2 experimented loss of mass due to the disaggregation of polymeric moieties from ferrogel structure. The methodology of magnetic nanoparticles incorporation directly influenced on the adsorption capacity of both ferrogels (FG1 and FG2). As it is shown in Figure 7, FG1 displayed maximum Cd adsorption at this pH value.

During the first 60 min, the swelling degree of FG1 was markedly higher (over 20–50%) than FG2 (Figure 6). This fact facilitated metal diffusion inside the ferrogel. As the ferrogel absorbs water, it could absorb metal ions, too. Similar results found by Paulino et al. [41] in hydrogel based on chitosan, gum Arabic, and maltodextrin. The authors attributed the significant cadmium ion removal from the solution to the phenomenon of partition.

4.10.2. Kinetics of adsorption

Figure 7b displays the cadmium ion adsorption capacity as function of contact time using FG1 and FG2. An initial rapid adsorption is observed during the first 10 min, reaching the maximum adsorption capacity at 30 min of contact time as it can be observed from swelling assays, during this time, ferrogel reached the maximum water content. As it can be seen a higher Cd removal was achieved using FG1, where the maximum was about 35 mg g⁻¹ of ferrogel (corresponding to ~90% of available metal ion). As a difference, FG2 adsorbed a maximum of about 25 mg g⁻¹ (~80% of Cd ion available). It is worth noting that both FGs reached the maximum adsorption levels at 30 min of contact time. Longer adsorption times induced the gradual desorption and re-adsorption of the heavy metal, until a time of about 60 min where the adsorption value remained constant at 28 and 20 mg g⁻¹ for FG1 and FG2, respectively. A maximum Cd adsorption of 50 mg g⁻¹ was reported by Paulino et al. [41] using chitosan and gum Arabic magnetic hydrogel, and 22 mg g⁻¹ using maltodextrin magnetic hydrogel. Other authors found a maximum of cadmium adsorption of about ~90%, performing the assay between 30 and 60 min and using poly(acrylonitrile-co-acrylic acid) magnetic hydrogel. The adsorption level remained constant until 204 min. These authors established that at long adsorption times the surface sites were saturated. In such conditions,

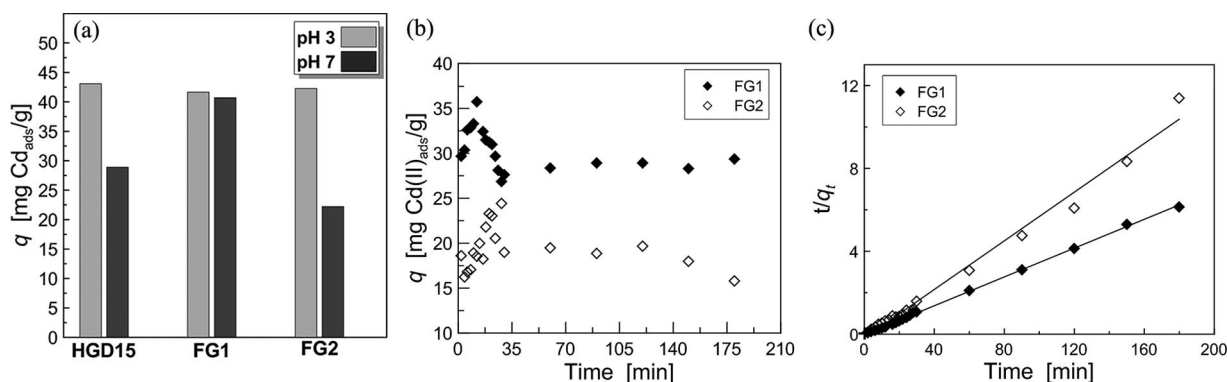


Figure 7. (a) Effect of pH on Cd adsorption on HGD15 and ferrogels (adsorbent dose: 20 mg, 20 mg L⁻¹, time: 2 h), (b) Effect of contact time (adsorbent dose: 100 mg, 100 mL, 100 mg L⁻¹, pH 7, time: 3 h), and (c) pseudo-second-order kinetic for Cd adsorption on FG1 and FG2. Note: HGD, gelatin-dextrose hydrogel.

Table 2. Characteristic parameters of applied kinetic models.

Sample	q_{exp}	Pseudo-first order		Pseudo-second order		q_e^{thrit} (mg g^{-1})
		k_1 (min^{-1})	R^2	k_2 $\text{g mg}^{-1} \text{min}^{-1}$	R^2	
FG1	28.46	0.1313	0.0455	0.0611	0.9992	28.74
FG2	18.37	0.2798	0.0744	0.0179	0.9876	17.0358

the rate of uptake was controlled by the rate at which the adsorbate was transported from the solution to the interior sites of the adsorbent [42]. As well as Hua et al. [43] obtained a maximum 17.7 mg Cd/g, using Fe_3O_4 -poly(L-cysteine/2-hydroxyethyl acrylate) hydrogel. In that case, the equilibrium time was reached at 24 h. The mechanism of adsorption was ascribed to a combination $-\text{NH}_2$ (of cysteine) and ion-exchange promoted by $-\text{SH}$ functional groups.

In this work, the fast initial adsorption of cadmium ions could be attributed to many available surface sites of the ferrogel such as amine and carboxyl, according to the data provided in Section 2a [38]. As it can be seen from Figure 7a, similar adsorption behavior was observed when comparing the adsorption assays at pH 7 for HG and FG1. Therefore, the extra advantage related to the use of ferrogel instead hydrogel is associated with the ability to easily remove the adsorbent by an external magnetic field.

In the case of FG2, a partial loss of stability was further observed at the end of the assay. In fact, the adsorbent could not be recuperated from the adsorption media in adequate conditions to be reutilized. This behavior is in accordance with swelling data discussed in previous section. For this reason, FG1 was selected to perform the following adsorption experiences.

The dependence of the adsorption as a function of the time was evaluated by pseudo-first-order and pseudo-second-order kinetic models; and the obtained plots are displayed in Figure 7c. The values of k_1 , k_2 , and correlation coefficients R^2 from Figure 7c are presented in Table 2. The correlation coefficient for pseudo-first-order is lower than the corresponding to pseudo-second-order model, which suggest that the kinetic behavior of ferrogels followed pseudo-second-order kinetic model. Hence, chemisorption was believed to be the rate limiting step. The kinetic behavior here observed was reported by other authors using similar adsorbent materials

[26]. Moreover, in own previous published research, we found the same trend for Cd adsorption on chitosan magnetic nanocomposites [39].

4.10.3. Adsorption isotherms

To explain the interaction between the adsorbate and the adsorbent material, adsorption isotherms are widely used and decisive in the optimum use of the adsorbent in the experimental conditions used [26,44]. For this, Langmuir and Freundlich isotherm models were commonly used to describe the equilibrium adsorption of metal ions by different adsorbents. For the adsorption isotherms of Cd(II) by FG1, the heavy metal ion concentration was varied between 0.5 and 400 mg mL^{-1} and contacted with 50 mg of adsorbent for 30 min at room temperature. Figure 8a displayed the Cd adsorption by ferrogel as function of heavy metal ion concentration.

The equation of Langmuir isotherm model, which describes the monolayer adsorption used is:

$$\frac{C_e}{q_e} = \left(\frac{C_e}{q_m} \right) + \frac{1}{q_m K_L} \quad (5)$$

where C_e (mg L^{-1}) is the equilibrium concentration of metal ions, q_e (mg g^{-1}) is the amount of heavy metal ions adsorbed per gram of ferrogel, q_m (mg/g) is the maximum adsorption of metal ions, and K_L (L mg^{-1}) is the Langmuir adsorption equilibrium constant.

For the Freundlich adsorption studies, the equation used was:

$$\log q_e = \log K_F + \frac{1}{n} \log C_e \quad (6)$$

where q_e (mg g^{-1}) is the adsorption capacity at equilibrium, C_e (mg L^{-1}) is the equilibrium concentration of cadmium ions in solution, and K_F and n are the physical constants of the Freundlich adsorption isotherm. Both parameters are indicators of the adsorption capacity and adsorption intensity, respectively.

The relative parameters calculated from the two kinetics models are listed in Table 3 and the fitted curves with the experimental data are shown in Figures 8b and 8c. From the correlation coefficients, it can be seen that the Freundlich (0.9806) model fits better than Langmuir model which has

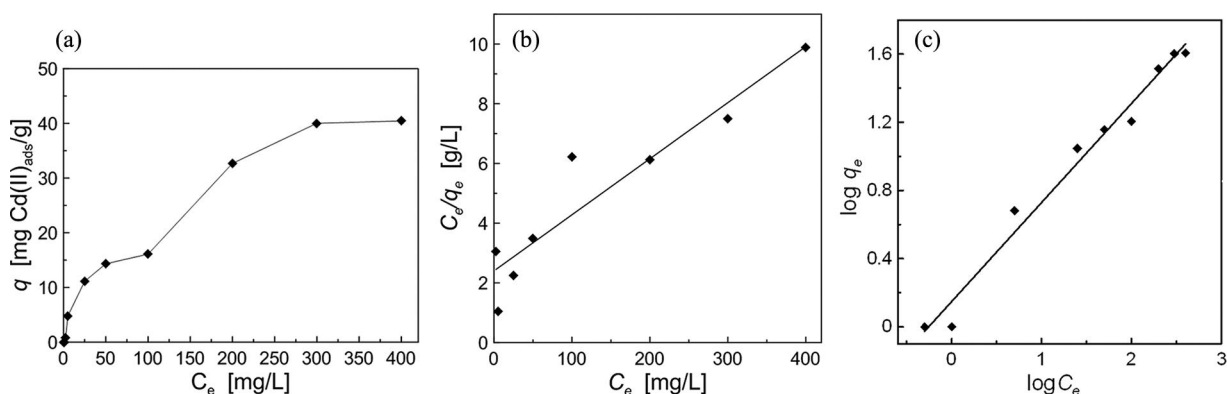


Figure 8. (a) Effect of initial concentration on the adsorption FG1 for Cd (II) (b) and (c) equilibrium isotherm analyses with the Langmuir and Freundlich models. Model parameters are provided in Table 3.

Table 3. Langmuir and Freundlich isotherm parameters for Cd(II) adsorption on ferrogel.

Langmuir constants			Freundlich constants		
q_m (mg g ⁻¹)	K_L (L mg ⁻¹)	R^2	K_F (mg g ⁻¹)	n	R^2
53.19	0.0078	0.8884	1.4090	1.7226	0.9806

the experimental data (0.8884). The n value higher than 1 supported the assumption that cadmium ion was adsorbed onto the ferrogel surface following the Freundlich model. Most of the research reported in the literature about adsorption capacities of hydro and ferrogel of gelatin followed Langmuir adsorption model [44]. This behavior is characteristic of monolayer adsorption. In this work, the synthesized ferrogel seems to have a heterogeneous surface, so the adsorption data were better adjusted by Freundlich model.

From the adsorption experiences developed above, the possible interactions between Cd(II) and the ferrogel could be described. The synthesized adsorbent materials are presented in sheet form where the magnetite nanoparticles are distributed in the gel matrix. For this reason, two possible mechanism of heavy metal removal could be achieved. First, it is known that the amine and carboxyl are the main functional groups present in gelatin molecular structure, so they could be responsible for cadmium binding. As it was earlier discussed, the adsorption capacity of ferrogel is affected by different pH values, so complex reactions could be achieved between cadmium ions and ferrogel surface. Similar behavior was previously reported in gelatin/Fe₃O₄ material synthesized by plasma treatment [44]. In this study, the authors postulated that in Fe₃O₄-g-gelatin, the amine and carboxyl groups of gelatin are responsible for Pb(II) binding. They attributed to the formation of surface complexes of Pb²⁺ ions with amine groups ((-NH₂)₂Pb²⁺) at low pH values and at high pH values. In such case, the removal of heavy metal ion by gelatin/Fe₃O₄ was mainly dominated by carboxyl groups interacting with heavy metal ions (COOPb(OH)). Based on previous studies of the authors, where analyzed the mechanism of heavy metal adsorption on chitosan/magnetite nanocomposites. These nanocomposites have amine and carboxyl groups in their structure similar as ferrogels. The amine groups are responsible for the heavy metal adsorption and the main mechanism proposed is the formation of covalent bonds between heavy metal and the adsorbent [40]. So in this study the authors propose the possible mechanism of heavy metal adsorption is through covalent bonds between amine groups of gelatin and heavy metal and the formation of metal/adsorbent complex. Second, due to the porosity of ferrogel, the capacity for heavy metal removal could be also attributed to metal ions diffusion into gel matrix and consequently could be retained into ferrogel structure. The proposal of absorption as other mechanism for heavy metal ion removal was proposed using magnetic hydrogels [37].

4.11. Desorption studies, regeneration of ferrogel, and reuse assays

The possibility to reuse the adsorbent is a key factor to take into account in the design of materials to water treatment

aiming to improve wastewater process, the economic aspects as well as practical implementation of these technologies. For the best of our knowledge, most of the literature reports the regeneration of magnetic hydrogel using acid solutions and/or a chelating agent to remove the heavy metal ion from the ferrogel matrix [43,45]. This aspect was evaluated using FG1 by performing sequential cycles of adsorption/desorption. The collected data are shown in Figure 9 in terms of the adsorption capability (expressed as mg Cd/g adsorbent) as a function of each cycle and the percentage of Cd removed from the solution after each cycle. Four consecutive adsorption-desorption-adsorption cycles were performed.

In the first adsorption assay, the adsorption capacity of FG1 was about 16 mg g⁻¹ approximately, retaining about 25% of cadmium available. It can be observed a decrease tendency on cadmium adsorption expressed as mg of heavy metal ion adsorbed per gram of adsorbent in each cycle of adsorption respect of the amount of heavy metal ion available in the solution. However, the final Cd concentration removed after the fourth assay was almost 14 mg g⁻¹, retaining more than 30% of heavy metal ion available. So the most promissory of these data is that these levels of adsorption were almost constant all along the cycles evaluated. It is important to highlight that between each cycle of reuse the ferrogel was washed several times (from 4 to 6 times) with distilled water.

The water samples remnant after washing were measured by atomic absorption spectroscopy to determine the Cd(II) concentration. The presence of Cd was confirmed but its quantification was not possible due to the lower concentrations that remained lower than the detection limit of the equipment.

Therefore, it may assume that any reduction on the efficiency, in terms of the adsorption capability of the material, occurred during the reutilization assays. It is noteworthy that any harmful eluents were used to remove heavy metal ions during material regeneration process. The washes only involved distilled water. Furthermore, and, as it was expected, the ferrogel remained stable in all the experiences, as it was previously revealed by the swelling assays against the time. Although it is true that during regeneration variable volumes of diluted cadmium solution may be produced; in this work, the assay was conducted to analyze the adsorption efficiency

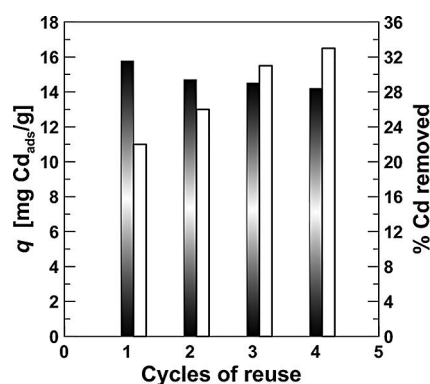


Figure 9. Cycles of Cd(II) adsorption on FG (adsorbent dose = 100 mg, initial conc. Of Cd(II) = 50 mg L⁻¹, pH = 7, contact time = 30 min, r.t.).

of ferrogel. In separate future works, the way to reduce and/or treat the remained residues will be addressed.

5. Conclusion

In this contribution, two different routes to obtain magnetic gels from gelatin and magnetite are presented. It was found that the most efficient synthetic route is the in situ co-precipitation of magnetite nanoparticles in the preformed hydrogel. In this case, a stable material with improved mechanical and swelling properties was obtained. Adsorption capability as well as gels stability and mechanical properties demonstrated to be highly dependent on the methodology of magnetite incorporation.

The objective of this study was to develop a reinforcement hydrogel structure with magnetic properties to be using for heavy metal adsorption in polluted water. For this purpose, the adsorption capacity of prepared materials was tested using one heavy metal as model. More studies are needed to evaluate adsorption performance under competitive adsorption conditions with various metals. Satisfactory adsorption performance was observed removing around 30% of heavy metal ion available using the adsorbent obtained by co-precipitation the iron oxide nanoparticles *in situ* in the polymer matrix. The ferrogel demonstrated to have great possibilities of reuse along four repeated adsorption cycles and the material regeneration was possible by only washing with distilled water, maintaining the adsorption performance.

The adsorbent materials proposed in this study represent an efficient, low cost, and easy handling alternative to the traditional tools used in water remediation. Besides, the here proposed materials constitute novel ones since the set of raw materials, procedures, and application have not been earlier reported according to the contributions in open literature.

Acknowledgments

The authors acknowledge the financial support of CONICET, ANPCyT (PICT 2013-1983) and the PGI N°24/ZQ09 (UNS, Argentina, Dra. Veronica Lassalle).

Funding

This work was supported by the Ministerio de Ciencia, Tecnología e Innovación Productiva [Grant Number PICT-2015- 0932] and Universidad Nacional del Sur [Grant Number PGI 24/ZQ09].

References

- [1] Ullah, F.; Othman, M. B. H.; Javed, F.; Ahmad, Z.; Md Akil, H. Classification, processing and application of hydrogels: A review. *Mater. Sci. Eng. C* **2015**, *57*, 414–433. doi:10.1016/j.msec.2015.07.053
- [2] Ahmed, E. M. Hydrogel: Preparation, characterization, and applications: A review. *J. Adv. Res.* **2015**, *6*, 105–121. doi:10.1016/j.jare.2013.07.006
- [3] Guilherme, M. R.; Reis, A. V.; Paulino, A. T.; Fajardo, A. R.; Muniz, E. C.; Tambourgi, E. B. Superabsorbent hydrogel based on modified polysaccharide for removal of Pb21 and Cu21 from water with excellent performance. *J. Appl. Polym. Sci.* **2007**, *105*, 2903–2909. doi:10.1002/app
- [4] Xie, J.; Zhang, H.; Li, X.; Shi, Y. Entrapment of methyl parathion hydrolase in cross-linked poly(γ -glutamic acid)/gelatin hydrogel. *Biomacromolecules*, *15*, 690–697.
- [5] Yang, L.; Li, X.; Li, X.; Su, Z.; Zhang, C.; Xu, M.; Zhang, H. Improved stability and enhanced efficiency to degrade chlorimuron-ethyl by the entrapment of esterase SulE in cross-linked poly(γ -glutamic acid)/gelatin hydrogel. *J. Hazard Mater.* **2015**, *287*, 287–295. doi:10.1016/j.jhazmat.2015.01.056
- [6] Paulino, A. T.; Guilherme, M. R.; Reis, A. V.; Campese, G. M.; Muniz, E. C.; Nozaki, J. Removal of methylene blue dye from an aqueous media using superabsorbent hydrogel supported on modified polysaccharide. *J. Colloid Interface Sci.* **2006**, *301*, 55–62. doi:10.1016/j.jcis.2006.04.036
- [7] Rathna, G. V. N. Gelatin hydrogels: Enhanced biocompatibility, drug release and cell viability. *J. Mater. Sci. Mater. Med.* **2008**, *19*, 2351–2358. doi:10.1007/s10856-007-3334-9
- [8] Lai, J. Y. Biocompatibility of chemically cross-linked gelatin hydrogels for ophthalmic use. *J. Mater. Sci. Mater. Med.* **2010**, *21*, 1899–1911. doi:10.1007/s10856-010-4035-3
- [9] Satapathy, S.; Singh, V. K.; Sagiri, S. S.; Agarwal, T.; Banerjee, I.; Bhattacharya, M. K.; Kumar, N.; Pal, K. Development and characterization of gelatin-based hydrogels, emulsion hydrogels, and bigels: A comparative study. *J. Appl. Polym. Sci.* **2015**, *132*, 1–12. doi:10.1002/app.41502
- [10] Sun, X.; Zhao, X.; Zhao, L.; Li, Q.; D’Ortenzio, M.; Nyugen, B.; Xu, X.; Wen, Y. Development of a hybrid gelatin hydrogel platform for tissue engineering and protein delivery applications. *J. Mater. Chem. B* **2015**, *3*, 6368–6376. doi:10.1039/c5tb00645g
- [11] Bigi, A.; Cojazzi, G.; Panzavolta, S.; Roveri, N.; Rubini, K. Stabilization of gelatin films by crosslinking with genipin. *Biomaterials* **2002**, *23*, 4827–4832. doi:10.1016/S0142-9612(02)00235-1
- [12] Talebian, A.; Kordestani, S.; Rashidi, A. The effect of glutaraldehyde on the properties of gelatin films. *Kem. Ind.* **2007**, *56*, 537–541.
- [13] Loth, T.; Hötzel, R.; Kascholke, C.; Anderegg, U.; Schulz-Siegmund, M.; Hacker, M. C. Gelatin-based biomaterial engineering with anhydride-containing oligomeric cross-linkers. *Biomacromolecules* **2014**, *15*, 2104–2118. doi:10.1021/bm500241y
- [14] Barbucci, R.; Pasqui, D.; Giani, G.; de Cagna, M.; Fini, M.; Giardino, R.; Atrei, A. A novel strategy for engineering hydrogels with ferromagnetic nanoparticles as crosslinkers of the polymer chains. Potential applications as a targeted drug delivery system. *Soft Matter* **2011**, *7*, 5558. doi:10.1039/c1sm05174a
- [15] Suh, S. K.; Chapin, S. C.; Hatton, T. A.; Doyle, P. S. Synthesis of magnetic hydrogel microparticles for bioassays and tweezer manipulation in microwells. *Microfluid Nanofluidics* **2012**, *13*, 665–674. doi:10.1007/s10404-012-0977-8
- [16] Liu, H.; Wang, C.; Gao, Q.; Chen, J.; Ren, B.; Liu, X.; Tong, Z. Facile fabrication of well-defined hydrogel beads with magnetic nanocomposite shells. *Int. J. Pharm.* **2009**, *376*, 92–98. doi:10.1016/j.ijpharm.2009.04.031
- [17] Bender, P.; Tschöpe A.; Birringer, R. Magnetization measurements reveal the local shear stiffness of hydrogels probed by ferromagnetic nanorods. *J. Magn. Mater.* **2014**, *372*, 187–194. doi:10.1016/j.jmmm.2014.07.067
- [18] Helminger, M.; Wu, B.; Kollmann, T.; Benke, D.; Schwahn, D.; Pipich, V.; Faivre, D.; Zahn, D.; Cölfen, H. Synthesis and characterization of gelatin-based magnetic hydrogels. *Adv. Funct. Mater.* **2014**, *24*, 3187–3196. doi:10.1002/adfm.201303547
- [19] Hu, S.-H.; Liu, T.-Y.; Liu, D.-M.; Chen, S.-Y. Nano-ferrosponges for controlled drug release. *J. Control. Release* **2007**, *121*, 181–189. doi:10.1016/j.jconrel.2007.06.002
- [20] Huang, L. Y.; Yang, M. C. Behaviors of controlled drug release of magnetic-gelatin hydrogel coated stainless steel for drug-eluting-stents application. *J. Magn. Mater.* **2007**, *310*, 2874–2876. doi:10.1016/j.jmmm.2006.11.151
- [21] Jayalekshmi, A. C.; Victor, S. P.; Sharma, C. P. Magnetic and degradable polymer/bioactive glass composite nanoparticles for biomedical applications. *Colloid Surf. B Biointerfaces* **2013**, *101*, 196–204. doi:10.1016/j.colsurfb.2012.06.027

- [22] Lassalle, V. L.; Zysler, R. D.; Ferreira, M. L. Novel and facile synthesis of magnetic composites by a modified co-precipitation method. *Mater. Chem. Phys.* **2011**, *130*, 624–634. doi:10.1016/j.matchemphys.2011.07.035
- [23] Ki, C. S.; Baek, D. H.; Gang, K. D.; Lee, K. H.; Um, I. C.; Park, Y. H. Characterization of gelatin nanofiber prepared from gelatin-formic acid solution. *Polymer (Guildf)* **2005**, *46*, 5094–5102. doi:10.1016/j.polymer.2005.04.040
- [24] Muyonga, J. H.; Cole, C. G. B.; Duodu, K. G. Fourier transform infrared (FTIR) spectroscopic study of acid soluble collagen and gelatin from skins and bones of young and adult Nile perch (*Lates niloticus*). *Food Chem.* **2004**, *86*, 325–332. doi:10.1016/j.foodchem.2003.09.038
- [25] Draye, J.-P.; Delaey, B.; van de Voorde, A.; van Den Bulcke, A.; Bogdanov, B.; Schacht, E. In vitro release characteristics of bioactive molecules from dextran dialdehyde cross-linked gelatin hydrogel film. *Biomaterials* **1998**, *19*, 99–107. doi:10.1016/S0142-9612(98)00049-0
- [26] Chen, G.; Qiao, C.; Wang, Y.; Yao, J. Synthesis of magnetic gelatin and its adsorption property for Cr(VI). *Ind. Eng. Chem. Res.* **2014**, *53*, 15576–15581. doi:10.1021/ie502709u
- [27] Sarika, P. R.; James, N. R. Preparation and characterisation of gelatin-gum arabic aldehyde nanogels via inverse miniemulsion technique. *Int. J. Biol. Macromol.* **2015**, *76*, 181–187. doi:10.1016/j.ijbiomac.2015.02.038
- [28] Dai, C. A.; Chen, Y. F.; Liu, M. W. Thermal properties measurements of renatured gelatin using conventional and temperature modulated differential scanning calorimetry. *J. Appl. Polym. Sci.* **2006**, *99*, 1795–1801. doi:10.1002/app.22711
- [29] Tseretely, G. I.; Smirnova, O. I. DSC study of melting; & glass transition in gelatins. *J. Therm. Anal.* **1992**, *38*, 1189–1201. doi:10.1007/BF01979179
- [30] Dai, C. A.; Liu, M. W. The effect of crystallinity and aging enthalpy on the mechanical properties of gelatin films. *Mater. Sci. Eng. A* **2006**, *423*, 121–127. doi:10.1016/j.msea.2005.10.082
- [31] Fraga, A. N.; Williams, R. J. J. Thermal properties of gelatin films. *Polymer (Guildf)* **1985**, *26*, 113–118. doi:10.1016/0032-3861(85)90066-7
- [32] Zheng, J. P.; Li, P.; Ma, Y. L.; Yao, K. D. Gelatin/montmorillonite hybrid nanocomposite. I. Preparation and properties. *J. Appl. Polym. Sci.* **2002**, *86*, 1189–1194. doi:10.1002/app.11062
- [33] Juríková, A.; Csach, K.; Koneracká, M.; Závášová, V.; Kubovčíková, M.; Kopčanský, P. Thermal analysis of magnetic nanoparticles modified with dextran. *Acta Phys. Pol. A* **2012**, *121*, 1296–1298.
- [34] Toledo Hijo, A. A. C.; da Costa, J. M. G.; Silva, E. K.; Azevedo, V. M.; Yoshida, M. I.; Borges, S. V. Physical; and thermal properties of oregano (*Origanum vulgare* L.) essential oil microparticles. *J. Food Process. Eng.* **2015**, *38*, 1–10. doi:10.1111/jfpe.12120
- [35] Goiti, E.; Salinas, M. M.; Arias, G.; Puglia, D.; Kenny, J. M.; Mijangos, C. Effect of magnetic nanoparticles on the thermal properties of some hydrogels. *Polym. Degrad. Stab.* **2007**, *92*, 2198–2205. doi:10.1016/j.polyimdegradstab.2007.02.025
- [36] Draye, J. P.; Delaey, B.; van de Voorde, A.; van Den Bulcke, A.; de Reu, B.; Schacht, E. In vitro and in vivo biocompatibility of dextran dialdehyde cross-linked gelatin hydrogel films. *Biomaterials* **1998**, *19*, 1677–1687. doi:10.1016/S0142-9612(98)00049-0
- [37] Ozay, O.; Ekici, S.; Baran, Y.; Kubilay, S.; Aktas, N.; Sahiner, N. Utilization of magnetic hydrogels in the separation of toxic metal ions from aqueous environments. *Desalination* **2010**, *260*, 57–64. doi:10.1016/j.desal.2010.04.067
- [38] Ozay, O.; Ekici, S.; Baran, Y.; Aktar, N.; Sahiner, N. Removal of toxic metal ions with magnetic hydrogels. *Water Res.* **2009**, *43*, 4403–4411. doi:10.1016/j.watres.2009.06.058
- [39] Horst, M. F.; Alvarez, M.; Lassalle, V. L. Removal of heavy metals from wastewater using magnetic nanocomposites: Analysis of the experimental conditions. *Sep. Sci. Technol.* **2016**, *51*, 550–563. doi:10.1080/01496395.2015.1086801
- [40] Duconseille, A.; Astruc, T.; Quintana, N.; Meersman, F.; Sante-Lhoutellier, V. Gelatin structure and composition linked to hard capsule dissolution: A review. *Food Hydrocoll.* **2015**, *43*, 360–376. doi:10.1016/j.foodhyd.2014.06.006
- [41] Paulino, A. T.; Belfiore, L. A.; Kubota, L. T.; Muniz, E. C. Efficiency of hydrogels based on natural polysaccharides in the removal of Cd²⁺ ions from aqueous solutions. *Chem. Eng. J.* **2011**, *168*, 68–76. doi:10.1016/j.cej.2010.12.037
- [42] Tiwari, A.; Sharma, N. Kinetic; & thermodynamic studies of adsorption of Cd²⁺ by superparamagnetic nano iron oxide-loaded poly (acrylonitrile-co-acrylic acid) hydrogel. *Res. Chem. Intermed.* **2015**, *41*, 2043–2062. doi:10.1007/s11164-013-1330-x
- [43] Hua, R.; Li, Z. Sulfhydryl functionalized hydrogel with magnetism: Synthesis, characterization, and adsorption behavior study for heavy metal removal. *Chem. Eng. J.* **2014**, *249*, 189–200. doi:https://doi.org/10.1016/j.cej.2014.03.097
- [44] Ren, X.; Yang, S.; Shao, D.; Tan, X. Retention of Pb(II) by a Low-cost magnetic composite prepared by environmentally-friendly plasma technique. *Sep. Sci. Technol.* **2013**, *48*, 1211–1219. doi:10.1080/01496395.2012.726307
- [45] Mahmoud, G. A. Adsorption of copper(II), lead(II), and cadmium(II) ions from aqueous solution by using hydrogel with magnetic properties. *Monatsh. Chem.* **2013**, *144*, 1097–1106. doi:10.1007/s00706-013-0957-z